

A Star Cluster Population of High Mass Black Hole Mergers in Gravitational Wave Data

Fabio Antonini,¹ Isobel M. Romero-Shaw,^{2,3} and Thomas Callister⁴

¹*Gravity Exploration Institute, School of Physics and Astronomy, Cardiff University, Cardiff, CF24 3AA, UK*

²*DAMTP, Centre for Mathematical Sciences, University of Cambridge, Wilberforce Road, Cambridge, CB3 0WA, UK*

³*Kavli Institute for Cosmology, Madingley Road, Cambridge, CB3 0HA, United Kingdom*

⁴*Kavli Institute for Cosmological Physics, The University of Chicago, Chicago, IL 60637, USA*

(Dated: June 28, 2024)

Stellar evolution theories predict a gap in the black hole birth mass spectrum as the result of pair instability processes in the cores of massive stars. This gap, however, is not seen in the binary black hole masses inferred from gravitational wave data. One explanation is that black holes form dynamically in dense star clusters where smaller black holes merge to form more massive black holes, populating the mass gap. We show that this model predicts a distribution of the effective and precessing spin parameters, χ_{eff} and χ_{p} , within the mass gap that is insensitive to assumptions about black hole natal spins. We analyze the distribution of χ_{eff} as a function of primary mass for the black hole binaries in the third gravitational wave transient catalog. We infer the presence of a high-mass population of black holes that is consistent with hierarchical formation in dense star clusters. This population becomes dominant above $44_{-4}^{+6}M_{\odot}$, which we interpret as the lower edge of the pair-instability mass gap. Upcoming data will enable us to tightly constrain the hierarchical formation hypothesis and refine our understanding of binary black hole formation.

Introduction. Observations of gravitational waves (GWs) from binary black hole (BH) mergers provides an unprecedented window into the astrophysics of massive stars [1–7]. However, our ability to learn from these detections is hindered by uncertainties in the theory of massive binary star evolution and BH formation, and the dependence of model results on initial conditions and parameters [e.g., 8–11]. One of these uncertainties is the location (and presence) of a mass gap in the BH birth mass distribution due to (pulsational) pair instability supernovae ((P)PISN), estimated to begin in the ~ 40 – $70M_{\odot}$ range and ending at $\sim 130M_{\odot}$ [12–15]. Such a gap is not observed in the BH mass distribution [6, 16]. If such a gap exists, then the formation of BHs within the mass gap can nevertheless be explained by scenarios involving dynamical interactions in dense star clusters or AGN disks, where BHs can grow through hierarchical mergers [17–24]. The detection of this high mass population will shed light on the origin of binary BH mergers as well as on the location of the (P)PISN mass gap.

The most precisely measured spin parameter from GW data is the effective inspiral spin χ_{eff} , a combination of the two component spins projected parallel to the orbital angular momentum [25]. Previous work has shown that the distribution of χ_{eff} can give important insights on the origin of the detected BH binary population [26–34]. The distribution of individual BH spins and of the precessing spin parameter χ_{p} [35] have also been leveraged in attempts to identify a dynamically-formed population in the data [30, 36–41], and correlations between BH spins and binary mass ratio [6, 28, 42–45] and possibly redshift [45, 46] have been inferred from the data. Other studies have examined possible relationships between BH mass and spin, as would be expected from a population

of hierarchical mergers [31, 34, 38, 39, 43, 46, 47]; thus far, evidence for any correlation between BH masses and spins has been tentative, with different studies yielding different conclusions. A clear detection of the (P)PISN mass gap and a population of hierarchical mergers remains elusive.

Here, we study the χ_{eff} and χ_{p} distributions as a function of primary BH mass m_1 to identify signatures of hierarchically formed BHs in the third gravitational wave transient catalog (GWTC-3). Using Bayesian inference, and simple but robust astrophysical models, we identify evidence for a population of high-mass BHs consistent with hierarchical formation, and place constraints on the existence and location of the (P)PISN gap in the mass spectrum of observed BHs.

Analytical model. We consider the spin parameters χ_{eff} and χ_{p} for a dynamically assembled BH merger population, in which the primary is a second-generation (2G) BH formed via an earlier merger and the secondary is a first-generation (1G) BH representing the direct end product of stellar evolution. The effective inspiral spin is defined as $\chi_{\text{eff}} = (m_1 a_1 \cos \theta_1 + m_2 a_2 \cos \theta_2) / (m_1 + m_2)$ [48, 49], and the effective precessing spin parameter is $\chi_{\text{p}} = \max \left(a_1 \sin \theta_1, \frac{3+4q}{4+3q} q a_2 \sin \theta_2 \right)$ [50, 51], where $q = m_2/m_1$ denotes the binary mass ratio, a_1 and a_2 are the dimensionless component spin magnitudes, and θ_1 and θ_2 are the angles between each spin vector and the orbital angular momentum.

For dynamical formation in a dense star cluster, we expect that [i] spin and orbital angular momenta are isotropically oriented [52]. For 1G+2G mergers we also expect: [ii] $a_1 = \tilde{a} \simeq 0.69$, in line with predictions from numerical-relativity simulations [53]; [iii] $a_1 \gg a_2$, as

a significant 1G+2G merger rate requires that BHs are formed with small spin, allowing for a higher cluster retention probability of merger remnants [19, 22]; and [iv] $m_1 \simeq 2m_2$, based on dynamical selection favouring the high-mass end of the BH mass function for both BH primary progenitors and for the secondary BH [54].

Given the above considerations, we expect that the most likely values of the spin parameters for a 1G+2G mergers are $\chi_{\text{eff}} \simeq \frac{\tilde{a}}{1.5} \cos \theta_1$ and $\chi_p \simeq \tilde{a} \sin \theta_1$, leading to the mean relation $\chi_p = \sqrt{\tilde{a}^2 - (1.5\chi_{\text{eff}})^2}$. Isotropy then implies a uniform distribution for χ_{eff} within $|\chi_{\text{eff}}| < \tilde{a}/1.5 \simeq 0.47$, and $p(\chi_p) \propto \frac{\chi_p}{\sqrt{\tilde{a}^2 - \chi_p^2}}$. Integrating, we find the cumulative spin distribution functions for 1G+2G mergers:

$$N_{12}(\leq \chi_{\text{eff}}) = 0.5 + 0.75 \frac{\chi_{\text{eff}}}{\tilde{a}}, \quad (1)$$

and

$$N_{12}(\leq \chi_p) = 1 - \sqrt{1 - \frac{\chi_p^2}{\tilde{a}^2}}. \quad (2)$$

For 2G+2G mergers, the probability density of χ_{eff} is obtained from the convolution of two uniform distributions, which gives $p(\chi_{\text{eff}}) \propto (\tilde{a} + \chi_{\text{eff}})$ for $\chi_{\text{eff}} \leq 0$ and $p(\chi_{\text{eff}}) \propto (\tilde{a} - \chi_{\text{eff}})$ for $\chi_{\text{eff}} > 0$. The corresponding cumulative distribution is

$$N_{22}(\leq \chi_{\text{eff}}) = \begin{cases} \frac{\chi_{\text{eff}}}{\tilde{a}} + \frac{1}{2} \frac{\chi_{\text{eff}}^2}{\tilde{a}^2} + \frac{1}{2} & \text{if } \chi_{\text{eff}} \leq 0 \\ \frac{\chi_{\text{eff}}}{\tilde{a}} - \frac{1}{2} \frac{\chi_{\text{eff}}^2}{\tilde{a}^2} + \frac{1}{2} & \text{if } \chi_{\text{eff}} > 0. \end{cases} \quad (3)$$

Since θ_1 and θ_2 are independent, the distribution of χ_p is obtained by the product of the distributions for each of the two angles:

$$N_{22}(\leq \chi_p) = \left(1 - \sqrt{1 - \frac{\chi_p^2}{\tilde{a}^2}} \right)^2. \quad (4)$$

While the actual spin parameter distributions depend on the precise spin distribution of 1G BHs and binary mass ratios, we find that their impact is small, allowing for a precise and simple approximation.

To demonstrate the accuracy of our analytical predictions, we compare them to the results of globular cluster models evolved using the fast cluster code **cBHBd** [55]. Unless specified otherwise, our initial conditions and numerical modelling are the same as in [22]. In all models considered here we adopt an initial cluster half-mass density $\rho_h = 10^5 M_\odot \text{pc}^{-3}$ and the delayed supernova mechanism from [56].

We report the results from four models that differ by the choice of the initial BH spin distributions and the maximum mass of 1G BHs, m_{cut} . In one model, the initial BH spins are all set to zero and $m_{\text{cut}} \simeq 70M_\odot$. In the other three models, we assume that $m_{\text{cut}} \simeq 50M_\odot$

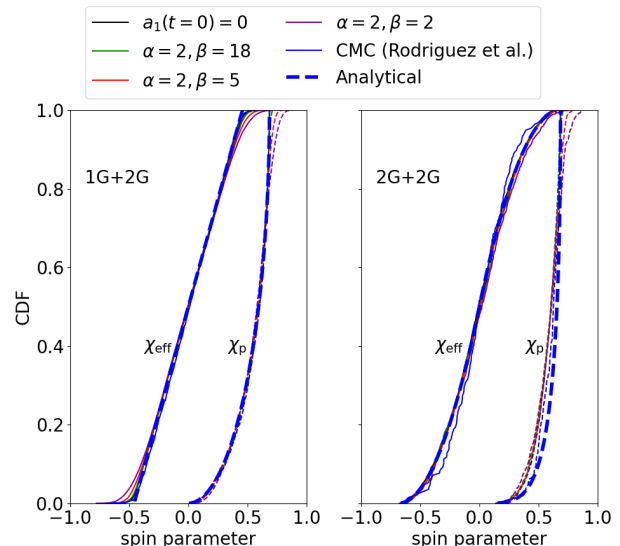


FIG. 1. Comparison between the CDF of χ_{eff} and χ_p obtained from our cluster models and the expected CDFs based on our analytical approximations. The lines are hard to distinguish because they lie on top of each other, showing the independence of these distributions on model assumptions and initial conditions.

and that the BH spin distribution follows a beta distribution with shape parameters $(\alpha, \beta) = (2, 18)$, $(2, 5)$ and $(2, 2)$; these distributions peak at $\simeq 0.06$, 0.2 , 0.5 and their corresponding median values are $\simeq 0.1$, 0.26 and 0.5 , respectively. All but the last model (with the highest spins) give differential merger rates at primary masses above m_{cut} consistent with those measured from LIGO/Virgo data. Above this mass, the merger rate is dominated by 1G+2G mergers in all models (see the Supplementary Material; SM).

In Fig. 1 we show the cumulative distributions of χ_{eff} and χ_p for 1G+2G and 2G+2G mergers, as well as the analytical predictions based on equations (1), (2), (3) and (4), and the spin parameter distributions from the cluster Monte Carlo models of [19]. The match with our expected distribution is good for all models. We note that although the simulated distributions become broader as the initial BH spins are increased, higher spins tend to reduce the merger rate below the one inferred from the data above m_{cut} , due to increased BH ejection from their host clusters. Thus, if hierarchical mergers are the most common class of binary BH merger above some threshold mass, our models predict a near-universal spin distribution, simply represented by equations (1) and (2). In the following, we test this prediction against GW data.

Bayesian inference. Since the value of χ_p is generally less well-measured in GW observations than χ_{eff} [4, 7], we predominantly consider hierarchical inference of the effective spin distribution. For this study, we use the subset of BHs from GWTC-3 with false alarm rates below

1 yr⁻¹ (see SM for more details). This results in a total of 69 binary BHs in our sample. In parallel with χ_{eff} , we hierarchically fit the distribution of q , m_1 , and redshift z as described in the SM. We incorporate selection effects using the set of successfully recovered binary BH injections provided by the LIGO-Virgo-KAGRA Collaboration and spanning their first three observing runs [6, 57].

We fit the χ_{eff} distribution to a mixture model comprising a Gaussian distribution, representing the bulk of the population at $m_1 \lesssim \tilde{m}$, and a uniform distribution, representing the population of 1G+2G hierarchical mergers at $m_1 \gtrsim \tilde{m}$, where \tilde{m} is the value of m_1 at which the transition between the Gaussian and uniform descriptions of χ_{eff} occurs:

$$\pi_{\mathcal{N}+\mathcal{U}}(\chi_{\text{eff}}|m_1) = \begin{cases} \mathcal{N}(\chi_{\text{eff}}; \mu, \sigma) & (m_1 < \tilde{m}) \\ \mathcal{U}(\chi_{\text{eff}}; w = 0.47) & (m_1 \geq \tilde{m}). \end{cases} \quad (5)$$

Here, $\mathcal{N}(\chi_{\text{eff}}; \mu, \sigma)$ denotes a normalized Gaussian distribution with mean μ and standard deviation σ truncated within $[-1, 1]$, and $\mathcal{U}(\chi_{\text{eff}}; w)$ is a uniform distribution defined over the range $|\chi_{\text{eff}}| < w$. We set $w = 0.47$, as predicted for hierarchical mergers. We use broad uninformative priors; the prior on \tilde{m} is uniform between 20 and $100M_{\odot}$. For more details on the implementation of the models and prior assumptions see the SM.

We consider additional models with increased complexity. Our second model, $\pi_{\mathcal{N}+\mathcal{U}_w}(\chi_{\text{eff}}|m_1)$, is similar to $\pi_{\mathcal{N}+\mathcal{U}}$, but with w now being a parameter that we infer from the data. The third model is

$$\begin{aligned} & \pi_{\mathcal{N}+\mathcal{N}\mathcal{U}_w}(\chi_{\text{eff}}|m_1) \\ &= \begin{cases} \mathcal{N}(\chi_{\text{eff}}; \mu, \sigma) & (m_1 < \tilde{m}) \\ \zeta \mathcal{U}(\chi_{\text{eff}}; w) + (1 - \zeta) \mathcal{N}_{\text{u}}(\chi_{\text{eff}}; \mu_{\text{u}}, \sigma_{\text{u}}) & (m_1 \geq \tilde{m}), \end{cases} \end{aligned} \quad (6)$$

where the mixing fraction $0 \leq \zeta \leq 1$. In this latter model, the potentially asymmetric distribution of χ_{eff} above \tilde{m} (if μ_{u} is non-zero) allows us to assess how well the data support the theoretical expectation of the symmetry of χ_{eff} around zero for $m_1 > \tilde{m}$ without this being enforced by the model.

If \tilde{m} cannot be constrained or its posterior distribution rails against the limits of the prior, this implies that a model with a separate spin distribution population above \tilde{m} cannot be statistically distinguished from a Gaussian model applied across the mass range. A well-measured \tilde{m} , in turn, instead implies that there is a distinct mass threshold above which the population of binary BH mergers has a measurably distinct distribution of χ_{eff} . We measure $\tilde{m} = 44_{-4}^{+6} M_{\odot}$ for the $\pi_{\mathcal{N}+\mathcal{U}}$ model (hereafter, reported measurements are median and 90% credible interval), implying that the data provide sufficient evidence to prefer the hierarchical model over the Gaussian model above this value. The posterior distributions of \tilde{m} and w are shown in Fig. 2. We infer $w = 0.5_{-0.2}^{+0.3}$ and $0.5_{-0.3}^{+0.3}$ under the $\pi_{\mathcal{N}+\mathcal{U}_w}$ and the $\pi_{\mathcal{N}+\mathcal{N}\mathcal{U}_w}$ models, respectively.

While the recovered posteriors on w are quite broad, they peak close to the expected value $w \simeq 0.47$ for hierarchical mergers. We show in Fig. 2 the cumulative distribution of χ_{eff} as inferred under $\pi_{\mathcal{N}+\mathcal{N}\mathcal{U}_w}$. Below \tilde{m} the distribution is a narrow Gaussian with mean $\mu = 0.05_{-0.04}^{+0.03}$; above \tilde{m} the distribution is consistent with being symmetric around zero, and its width is as expected from a hierarchically formed population of mergers.

Ref. [46] identified a systematic broadening in the distribution of χ_{eff} with increasing mass and/or redshift. The behavior we identify in this work – the transition to a broad χ_{eff} distribution above $\approx 45 M_{\odot}$ – is likely responsible for this conclusion. To verify this, we repeat our analysis with a fourth model, in which the fixed Gaussian spin distribution below \tilde{m} is replaced with one whose mean and variance evolve linearly with primary mass, as in [46]:

$$\begin{aligned} & \pi_{\mathcal{N}_m+\mathcal{U}_w}(\chi_{\text{eff}}|m_1) = \\ & \begin{cases} \mathcal{N}(\chi_{\text{eff}}; \mu_{\chi}(m_1), \sigma_{\chi}(m_1)) & (m_1 < \tilde{m}) \\ \mathcal{U}(\chi_{\text{eff}}; w) & (m_1 \geq \tilde{m}) \end{cases} \end{aligned} \quad (7)$$

where $\mu_{\chi}(m_1) = \mu + \delta\mu(m_1/10 M_{\odot} - 1)$ and $\log \sigma_{\chi}(m_1) = \log \sigma + \delta \log \sigma(m_1/10 M_{\odot} - 1)$. Under the $\pi_{\mathcal{N}_m+\mathcal{U}_w}$ model we infer that mean and variance of effective spins below \tilde{m} are now consistent with no or mild change with mass ($\delta\mu = 0.00_{-0.02}^{+0.02}$, $\delta \log \sigma = -0.24_{-0.07}^{+0.22}$). In fact, the data prefer a reversal of the trend inferred in previous work [46], with the χ_{eff} distribution slightly narrowing with mass below \tilde{m} . Our interpretation is that the population above \tilde{m} may drive the mass/redshift-dependent broadening reported in [46].

Finally, we consider a model where we also fit for the distribution of χ_{p} , which is represented by a mixture of two Gaussian distributions truncated within $[0, 1]$, one below and one above \tilde{m} :

$$\pi_{\chi_{\text{p}}}(\chi_{\text{eff}}|m_1) = \begin{cases} \mathcal{N}(\chi_{\text{eff}}; \mu, \sigma) \mathcal{N}(\chi_{\text{p}}; \mu_{\text{p,l}}, \sigma_{\text{p,l}}) & (m_1 < \tilde{m}) \\ \mathcal{U}(\chi_{\text{eff}}; w) \mathcal{N}(\chi_{\text{p}}; \mu_{\text{p,u}}, \sigma_{\text{p,u}}) & (m_1 \geq \tilde{m}) \end{cases} \quad (8)$$

Under this model, we infer $\tilde{m} = 46_{-4}^{+6} M_{\odot}$. We show the derived distribution of χ_{p} in Fig. 2. The distributions below and above \tilde{m} can be clearly distinguished and the latter is broadly consistent with the theoretical expectation.

Conclusions. We compare the predicted distribution of the effective spin parameters χ_{eff} and χ_{p} for hierarchical mergers to that of the population of observed BH binaries, finding evidence that the spin properties of observed binary BHs change at $\simeq 44 M_{\odot}$. Above this mass, the χ_{eff} distribution supports the hypothesis of a (P)PISN gap in BH birth masses, which is repopulated by hierarchical mergers in dense clusters. Sequential mergers in triples or quadruples [58, 59] are also possible, though the expected low merger rate makes this less likely [60]. BHs

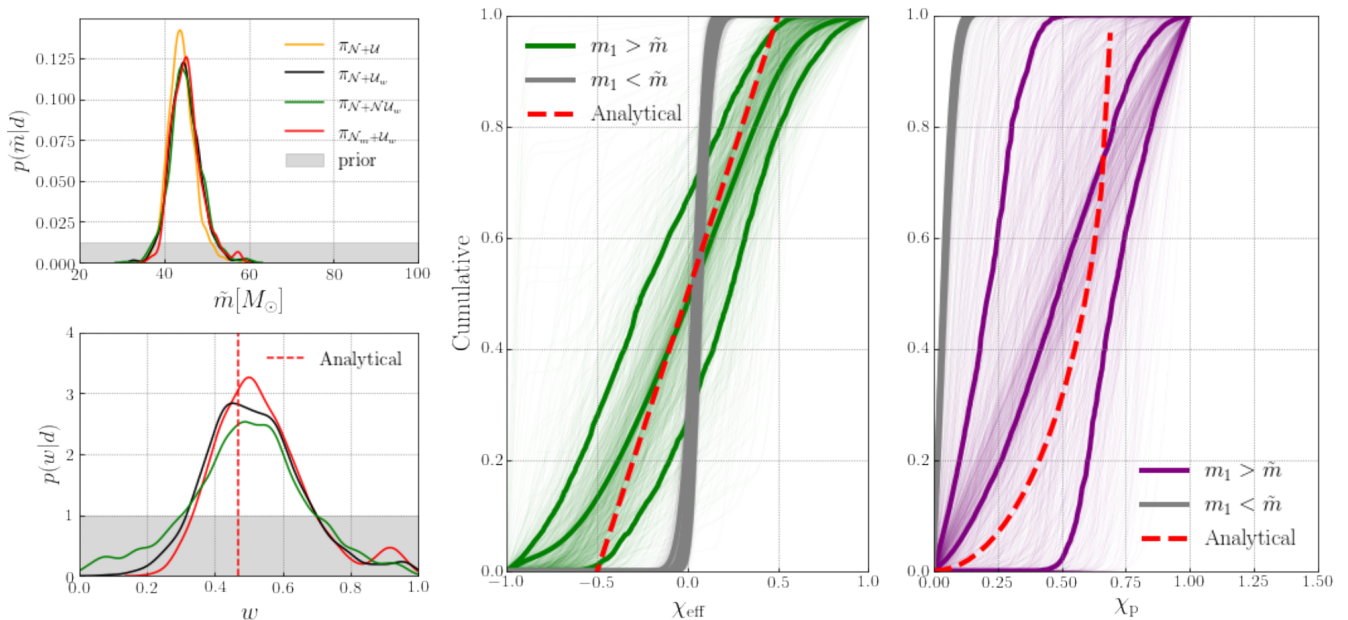


FIG. 2. Marginalised distributions of \tilde{m} (upper-left panel) and w (lower-left panel) obtained under the models described in the main text. The horizontal axes span the range of the assumed uniform priors as shown. The middle panel gives the cumulative distribution of χ_{eff} for the $\pi_{N+N\mathcal{U}_w}$ model, for both the Gaussian component at $m_1 \lesssim \tilde{m}$ and the Uniform+Gaussian component at $m_1 \gtrsim \tilde{m}$. The grey region shows the prior on each parameter. In the right panel we show the cumulative distribution of χ_p when fitting for both χ_p and χ_{eff} using equation (8). Thick lines show the median, 10th and 90th quantiles, while light lines correspond to individual draws from the posterior (PDFs are shown in the SM). Analytical predictions are from equation (1) and equation (2).

in the (P)PISN mass gap can also arise from gas accretion and/or hierarchical mergers in AGN disks [61, 62], and stellar mergers in star clusters [63, 64]. These latter scenarios are unlikely to give rise to the same χ_{eff} distributions as hierarchical BH mergers in clusters [24, 65, 66], and are therefore disfavored by our analysis as a primary formation mechanism.

The hierarchical formation hypothesis for high mass BHs makes other testable predictions that will enable tighter constraints from future GW observations with a growing population of BHs. In particular, it implies a large number of dynamically-formed 1G+1G mergers in the overall GW population. Therefore, a significant fraction of all the detected binaries should present a residual eccentric signature [67–69], of which traces are already claimed to exist in the data [70, 71]. Moreover, if mass-gap BHs form only through hierarchical mergers in clusters, we should expect $\sim 5\%$ of mass-gap mergers to be measurably eccentric. Additionally, because BHs with mass above $\sim 90M_\odot$ can only be formed from at least two previous mergers and these are rare, we might expect to find a drop/discontinuity in the inferred merger rate (and binary properties) near this mass.

Our results have important implications for our understanding of star clusters and BH formation. Ref. [22] showed that dynamical formation in globular clusters [72–74] can explain the inferred merger rate above \simeq

$30M_\odot$, including the extended high mass tail, if BHs are allowed to grow hierarchically. They showed, however, that this can only be achieved for cluster initial half-mass densities $\rho_h \gtrsim 10^4 M_\odot$ and if BHs are formed with small spins.

Acknowledgments. FA is supported by the UK’s Science and Technology Facilities Council grant ST/V005618/1. IMRS is supported by the Herchel Smith Postdoctoral Fellowship Fund. This material is based upon work supported by NSF’s LIGO Laboratory which is a major facility fully funded by the National Science Foundation, as well as the Science and Technology Facilities Council (STFC) of the United Kingdom, the Max-Planck-Society (MPS), and the State of Niedersachsen/Germany for support of the construction of Advanced LIGO and construction and operation of the GEO600 detector. Additional support for Advanced LIGO was provided by the Australian Research Council. Virgo is funded, through the European Gravitational Observatory (EGO), by the French Centre National de Recherche Scientifique (CNRS), the Italian Istituto Nazionale di Fisica Nucleare (INFN) and the Dutch Nikhef, with contributions by institutions from Belgium, Germany, Greece, Hungary, Ireland, Japan, Monaco, Poland, Portugal, Spain. KA-GRA is supported by Ministry of Education, Culture, Sports, Science and Technology (MEXT), Japan Society for the Promotion of Science (JSPS) in Japan; Na-

tional Research Foundation (NRF) and Ministry of Science and ICT (MSIT) in Korea; Academia Sinica (AS) and National Science and Technology Council (NSTC) in Taiwan. The authors are grateful for computational resources provided by Cardiff University and supported by STFC grant ST/V005618/1.

Main software: `astropy` [75]; `bilby` [76]; `cBHd` [55]; `jax` [77]; `numpy` [78]; `numpyro` [79, 80]; `scipy` [81].

Data and code availability. The cluster and hierarchical inference codes used to produce the results in this paper and the resulting data products are available under reasonable request.

-
- [1] Abbott et al., *Classical and Quantum Gravity* **32**, 074001 (2015), [arXiv:1411.4547 \[gr-qc\]](#).
- [2] Virgo Collaboration, *Classical and Quantum Gravity* **32**, 024001 (2015), [arXiv:1408.3978 \[gr-qc\]](#).
- [3] Abbott et al., *Phys. Rev. Lett.* **116**, 061102 (2016), [arXiv:1602.03837 \[gr-qc\]](#).
- [4] LIGO Scientific Collaboration and Virgo Collaboration, *ApJL* **882**, L24 (2019), [arXiv:1811.12940 \[astro-ph.HE\]](#).
- [5] Abbott et al., *Physical Review X* **9**, 031040 (2019), [arXiv:1811.12907 \[astro-ph.HE\]](#).
- [6] Abbott et al., *Physical Review X* **13**, 011048 (2023), [arXiv:2111.03634 \[astro-ph.HE\]](#).
- [7] Abbott et al., *Physical Review X* **13**, 041039 (2023), [arXiv:2111.03606 \[gr-qc\]](#).
- [8] F. Antonini and M. Gieles, *Phys. Rev. D* **102**, 123016 (2020), [arXiv:2009.01861 \[astro-ph.HE\]](#).
- [9] A. Olejak, K. Belczynski, and N. Ivanova, *A&A* **651**, A100 (2021), [arXiv:2102.05649 \[astro-ph.HE\]](#).
- [10] M. Zevin, S. S. Bavera, C. P. L. Berry, V. Kalogera, T. Fragos, P. Marchant, C. L. Rodriguez, F. Antonini, D. E. Holz, and C. Pankow, *Astrophys. J.* **910**, 152 (2021), [arXiv:2011.10057 \[astro-ph.HE\]](#).
- [11] F. S. Broekgaarden, E. Berger, S. Stevenson, S. Justham, I. Mandel, M. Chruślińska, L. A. C. van Son, T. Wagg, A. Vigna-Gómez, S. E. de Mink, D. Chattopadhyay, and C. J. Neijssel, *MNRAS* **516**, 5737 (2022), [arXiv:2112.05763 \[astro-ph.HE\]](#).
- [12] K. Belczynski, A. Heger, W. Gladysz, A. J. Ruitter, S. Woosley, G. Wiktorowicz, H. Y. Chen, T. Bulik, R. O’Shaughnessy, D. E. Holz, C. L. Fryer, and E. Berti, *A&A* **594**, A97 (2016), [arXiv:1607.03116 \[astro-ph.HE\]](#).
- [13] R. Farmer, M. Renzo, S. E. de Mink, M. Fishbach, and S. Justham, *ApJL* **902**, L36 (2020), [arXiv:2006.06678 \[astro-ph.HE\]](#).
- [14] L. A. C. van Son, S. E. De Mink, F. S. Broekgaarden, M. Renzo, S. Justham, E. Laplace, J. Morán-Fraile, D. D. Hendriks, and R. Farmer, *Astrophys. J.* **897**, 100 (2020), [arXiv:2004.05187 \[astro-ph.HE\]](#).
- [15] J. Ziegler and K. Freese, *Phys. Rev. D* **104**, 043015 (2021), [arXiv:2010.00254 \[astro-ph.HE\]](#).
- [16] B. Edelman, Z. Doctor, and B. Farr, *ApJL* **913**, L23 (2021), [arXiv:2104.07783 \[astro-ph.HE\]](#).
- [17] R. M. O’Leary, F. A. Rasio, J. M. Fregeau, N. Ivanova, and R. O’Shaughnessy, *Astrophys. J.* **637**, 937 (2006), [arXiv:astro-ph/0508224 \[astro-ph\]](#).
- [18] F. Antonini and F. A. Rasio, *Astrophys. J.* **831**, 187 (2016), [arXiv:1606.04889 \[astro-ph.HE\]](#).
- [19] C. L. Rodriguez, M. Zevin, P. Amaro-Seoane, S. Chatteerjee, K. Kremer, F. A. Rasio, and C. S. Ye, *Phys. Rev. D* **100**, 043027 (2019), [arXiv:1906.10260 \[astro-ph.HE\]](#).
- [20] H. Tagawa, B. Kocsis, Z. Haiman, I. Bartos, K. Omukai, and J. Samsing, *Astrophys. J.* **908**, 194 (2021), [arXiv:2012.00011 \[astro-ph.HE\]](#).
- [21] M. Mapelli, M. Dall’Amico, Y. Bouffanais, N. Giacobbo, M. Arca Sedda, M. C. Artale, A. Ballone, U. N. Di Carlo, G. Iorio, F. Santoliquido, and S. Torniamenti, *MNRAS* **505**, 339 (2021), [arXiv:2103.05016 \[astro-ph.HE\]](#).
- [22] F. Antonini, M. Gieles, F. Dosopoulou, and D. Chattopadhyay, *MNRAS* **522**, 466 (2023), [arXiv:2208.01081 \[astro-ph.HE\]](#).
- [23] S. Torniamenti, M. Mapelli, C. Périgois, M. Arca Sedda, M. C. Artale, M. Dall’Amico, and M. P. Vaccaro, *arXiv e-prints*, [arXiv:2401.14837 \(2024\)](#), [arXiv:2401.14837 \[astro-ph.HE\]](#).
- [24] M. P. Vaccaro, M. Mapelli, C. Périgois, D. Barone, M. C. Artale, M. Dall’Amico, G. Iorio, and S. Torniamenti, *A&A* **685**, A51 (2024), [arXiv:2311.18548 \[astro-ph.HE\]](#).
- [25] É. Racine, *Phys. Rev. D* **78**, 044021 (2008), [arXiv:0803.1820 \[gr-qc\]](#).
- [26] W. M. Farr, S. Stevenson, M. C. Miller, I. Mandel, B. Farr, and A. Vecchio, *Nature* **548**, 426 (2017).
- [27] B. Farr, D. E. Holz, and W. M. Farr, *The Astrophysical Journal* **854**, L9 (2018).
- [28] T. A. Callister, C.-J. Haster, K. K. Y. Ng, S. Vitale, and W. M. Farr, *ApJL* **922**, L5 (2021), [arXiv:2106.00521 \[astro-ph.HE\]](#).
- [29] C. Kimball, C. Talbot, C. P. L. Berry, M. Zevin, E. Thrane, V. Kalogera, R. Buscicchio, M. Carney, T. Dent, H. Middleton, E. Payne, J. Veitch, and D. Williams, *ApJL* **915**, L35 (2021), [arXiv:2011.05332 \[astro-ph.HE\]](#).
- [30] Y.-Z. Wang, Y.-J. Li, J. S. Vink, Y.-Z. Fan, S.-P. Tang, Y. Qin, and D.-M. Wei, *Astrophys. J. Lett.* **941**, L39 (2022), [arXiv:2208.11871 \[astro-ph.HE\]](#).
- [31] M. Fishbach, C. Kimball, and V. Kalogera, *ApJL* **935**, L26 (2022), [arXiv:2207.02924 \[astro-ph.HE\]](#).
- [32] T. A. Callister, S. J. Miller, K. Chatziioannou, and W. M. Farr, *ApJL* **937**, L13 (2022), [arXiv:2205.08574 \[astro-ph.HE\]](#).
- [33] J. Golomb and C. Talbot, *Phys. Rev. D* **108**, 103009 (2023), [arXiv:2210.12287 \[astro-ph.HE\]](#).
- [34] A. Ray, I. Magaña Hernandez, K. Breivik, and J. Creighton, *arXiv e-prints*, [arXiv:2404.03166 \(2024\)](#), [arXiv:2404.03166 \[astro-ph.HE\]](#).
- [35] P. Schmidt, F. Ohme, and M. Hannam, *Phys. Rev. D* **91**, 024043 (2015).
- [36] S. Vitale, R. Lynch, R. Sturani, and P. Graff, *Classical and Quantum Gravity* **34**, 03LT01 (2017), [arXiv:1503.04307 \[gr-qc\]](#).
- [37] C. Hoy, S. Fairhurst, M. Hannam, and V. Tiwari, *Astrophys. J.* **928**, 75 (2022), [arXiv:2110.13542 \[gr-qc\]](#).
- [38] M. Mould, D. Gerosa, and S. R. Taylor, *Phys. Rev. D* **106**, 103013 (2022), [arXiv:2203.03651 \[astro-ph.HE\]](#).
- [39] Y.-J. Li, Y.-Z. Wang, S.-P. Tang, and Y.-Z. Fan, *arXiv e-prints*, [arXiv:2303.02973 \(2023\)](#), [arXiv:2303.02973 \[astro-ph.HE\]](#).
- [40] Y.-J. Li, S.-P. Tang, S.-J. Gao, D.-C. Wu, and Y.-Z. Wang, *arXiv e-prints*, [arXiv:2404.09668 \(2024\)](#), [arXiv:2404.09668 \[astro-ph.HE\]](#).
- [41] G. Pierra, S. Mastrogiovanni, and S. Perriès, *arXiv e-*

- prints , arXiv:2406.01679 (2024), arXiv:2406.01679 [gr-qc].
- [42] C. Adamcewicz and E. Thrane, *MNRAS* **517**, 3928 (2022), arXiv:2208.03405 [astro-ph.HE].
- [43] V. Tiwari, *Astrophys. J.* **928**, 155 (2022), arXiv:2111.13991 [astro-ph.HE].
- [44] C. Adamcewicz, P. D. Lasky, and E. Thrane, *Astrophys. J.* **958**, 13 (2023), arXiv:2307.15278 [astro-ph.HE].
- [45] J. Heinzl, S. Biscoveanu, and S. Vitale, *Phys. Rev. D* **109**, 103006 (2024), arXiv:2312.00993 [astro-ph.HE].
- [46] S. Biscoveanu, T. A. Callister, C.-J. Haster, K. K. Y. Ng, S. Vitale, and W. M. Farr, *ApJL* **932**, L19 (2022), arXiv:2204.01578 [astro-ph.HE].
- [47] J. Godfrey, B. Edelman, and B. Farr, arXiv e-prints , arXiv:2304.01288 (2023), arXiv:2304.01288 [astro-ph.HE].
- [48] L. Santamaría, F. Ohme, P. Ajith, B. Brügmann, N. Dorband, M. Hannam, S. Husa, P. Mösta, D. Pollney, C. Reisswig, E. L. Robinson, J. Seiler, and B. Krishnan, *Physical Review D* **82**, 064016 (2010).
- [49] P. Ajith, M. Hannam, S. Husa, Y. Chen, B. Brügmann, N. Dorband, D. Müller, F. Ohme, D. Pollney, C. Reisswig, L. Santamaría, and J. Seiler, *Phys. Rev. Lett.* **106**, 241101 (2011), arXiv:0909.2867 [gr-qc].
- [50] M. Hannam, P. Schmidt, A. Bohé, L. Haegel, S. Husa, F. Ohme, G. Pratten, and M. Pürrer, *Phys. Rev. Lett.* **113**, 151101 (2014), arXiv:1308.3271 [gr-qc].
- [51] P. Schmidt, F. Ohme, and M. Hannam, *Phys. Rev. D* **91**, 024043 (2015), arXiv:1408.1810 [gr-qc].
- [52] C. L. Rodriguez, M. Zevin, C. Pankow, V. Kalogera, and F. A. Rasio, *ApJL*, In Press (2016), 10.3847/2041-8205/832/1/L2.
- [53] L. Rezzolla, E. Barausse, E. N. Dorband, D. Pollney, C. Reisswig, J. Seiler, and S. Husa, *Phys. Rev. D* **78**, 044002 (2008), arXiv:0712.3541 [gr-qc].
- [54] D. C. Heggie, *MNRAS* **173**, 729 (1975).
- [55] F. Antonini and M. Gieles, *MNRAS* **492**, 2936 (2020), arXiv:1906.11855 [astro-ph.HE].
- [56] C. L. Fryer, K. Belczynski, G. Wiktorowicz, M. Dominik, V. Kalogera, and D. E. Holz, *The Astrophysical Journal* **749**, 91 (2012).
- [57] The LIGO Scientific Collaboration, Virgo Collaboration, and KAGRA Collaboration, “GWTC-3: Compact Binary Coalescences Observed by LIGO and Virgo During the Second Part of the Third Observing Run — O1+O2+O3 Search Sensitivity Estimates,” (2021).
- [58] A. Vigna-Gómez, S. Toonen, E. Ramirez-Ruiz, N. W. C. Leigh, J. Riley, and C.-J. Haster, *ApJL* **907**, L19 (2021), arXiv:2010.13669 [astro-ph.HE].
- [59] B. Liu and D. Lai, *Monthly Notices of the Royal Astronomical Society* **502**, 2049 (2021), <https://academic.oup.com/mnras/article-pdf/502/2/2049/36204789/stab178.pdf>.
- [60] J. Stegmann, F. Antonini, and M. Moe, *MNRAS* **516**, 1406 (2022), arXiv:2112.10786 [astro-ph.SR].
- [61] I. Bartos, B. Kocsis, Z. Haiman, and S. Márka, *Astrophys. J.* **835**, 165 (2017), arXiv:1602.03831 [astro-ph.HE].
- [62] N. C. Stone, B. D. Metzger, and Z. Haiman, *MNRAS* **464**, 946 (2017), arXiv:1602.04226 [astro-ph.GA].
- [63] U. N. Di Carlo, M. Mapelli, Y. Bouffanais, N. Giacobbo, F. Santoliquido, A. Bressan, M. Spera, and F. Haardt, *MNRAS* **497**, 1043 (2020), arXiv:1911.01434 [astro-ph.HE].
- [64] U. N. Di Carlo, M. Mapelli, M. Pasquato, S. Rastello, A. Ballone, M. Dall’Amico, N. Giacobbo, G. Iorio, M. Spera, S. Torniamenti, and F. Haardt, *MNRAS* **507**, 5132 (2021), arXiv:2105.01085 [astro-ph.GA].
- [65] Y. Yang, I. Bartos, V. Gayathri, K. E. S. Ford, Z. Haiman, S. Klimentko, B. Kocsis, S. Márka, Z. Márka, B. McKernan, and R. O’Shaughnessy, *Phys. Rev. Lett.* **123**, 181101 (2019), arXiv:1906.09281 [astro-ph.HE].
- [66] G.-P. Li, D.-B. Lin, and Y. Yuan, *Phys. Rev. D* **107**, 063007 (2023).
- [67] F. Antonini, N. Murray, and S. Mikkola, *The Astrophysical Journal* **781**, 45 (2014).
- [68] J. Samsing, *Phys. Rev. D* **97**, 103014 (2018), arXiv:1711.07452 [astro-ph.HE].
- [69] C. L. Rodriguez, P. Amaro-Seoane, S. Chatterjee, and F. A. Rasio, *Phys. Rev. Lett.* **120**, 151101 (2018), arXiv:1712.04937 [astro-ph.HE].
- [70] I. Romero-Shaw, P. D. Lasky, and E. Thrane, *Astrophys. J.* **940**, 171 (2022), arXiv:2206.14695 [astro-ph.HE].
- [71] N. Gupte, A. Ramos-Buades, A. Buonanno, J. Gair, M. C. Miller, M. Dax, S. R. Green, M. Pürrer, J. Wildberger, J. Macke, and B. Schölkopf, arXiv e-prints , arXiv:2404.14286 (2024), arXiv:2404.14286 [gr-qc].
- [72] S. R. Kulkarni, P. Hut, and S. J. McMillan, *Nature* **364**, 421 (1993).
- [73] S. Sigurdsson and L. Hernquist, *Nature* **364**, 423 (1993).
- [74] S. F. Portegies Zwart and S. L. W. McMillan, *ApJL* **528**, L17 (2000), astro-ph/9910061.
- [75] P. Greenfield, T. Robitaille, E. Tollerud, T. Aldcroft, K. Barbary, P. Barrett, E. Bray, N. Crighton, A. Conley, S. Conseil, M. Davis, C. Deil, N. Dencheva, M. Droettboom, H. Ferguson, A. Ginsburg, F. Gröllier, H. Moritz Günther, C. Hanley, J. C. Hsu, W. Kerzendorf, R. Kramer, P. Lian Lim, D. Muna, P. Nair, A. Price-Whelan, D. Shiga, L. Singer, J. Taylor, J. Turner, J. Woillez, and V. Zabalza, “Astropy: Community Python library for astronomy,” *Astrophysics Source Code Library*, record ascl:1304.002 (2013).
- [76] G. Ashton, M. Hübner, P. D. Lasky, C. Talbot, K. Ackley, S. Biscoveanu, Q. Chu, A. Divakarla, P. J. Easter, B. Goncharov, F. Hernandez Vivanco, J. Harms, M. E. Lower, G. D. Meadors, D. Melchor, E. Payne, M. D. Pitkin, J. Powell, N. Sarin, R. J. E. Smith, and E. Thrane, *ApJS* **241**, 27 (2019), arXiv:1811.02042 [astro-ph.IM].
- [77] J. Bradbury, R. Frostig, P. Hawkins, M. J. Johnson, C. Leary, D. Maclaurin, G. Necula, A. Paszke, J. VanderPlas, S. Wanderman-Milne, and Q. Zhang, “JAX: composable transformations of Python+NumPy programs,” (2018).
- [78] C. R. Harris, K. J. Millman, S. J. van der Walt, R. Gommers, P. Virtanen, D. Cournapeau, E. Wieser, J. Taylor, S. Berg, N. J. Smith, R. Kern, M. Picus, S. Hoyer, M. H. van Kerkwijk, M. Brett, A. Haldane, J. F. del Río, M. Wiebe, P. Peterson, P. Gérard-Marchant, K. Shephard, T. Reddy, W. Weckesser, H. Abbasi, C. Gohlke, and T. E. Oliphant, *Nature (London)* **585**, 357 (2020), arXiv:2006.10256 [cs.MS].
- [79] D. Phan, N. Pradhan, and M. Jankowiak, arXiv e-prints , arXiv:1912.11554 (2019), arXiv:1912.11554 [stat.ML].
- [80] E. Bingham, J. P. Chen, M. Jankowiak, F. Obermeyer, N. Pradhan, T. Karaletsos, R. Singh, P. A. Szerlip, P. Horsfall, and N. D. Goodman, *J. Mach. Learn. Res.* **20**, 28:1 (2019).

- [81] P. Virtanen, R. Gommers, T. E. Oliphant, M. Haberland, T. Reddy, D. Cournapeau, E. Burovski, P. Peterson, W. Weckesser, J. Bright, S. J. van der Walt, M. Brett, J. Wilson, K. J. Millman, N. Mayorov, A. R. J. Nelson, E. Jones, R. Kern, E. Larson, C. J. Carey, Í. Polat, Y. Feng, E. W. Moore, J. VanderPlas, D. Laxalde, J. Perktold, R. Cimrman, I. Henriksen, E. A. Quintero, C. R. Harris, A. M. Archibald, A. H. Ribeiro, F. Pedregosa, P. van Mulbregt, and SciPy 1.0 Contributors, *Nature Methods* **17**, 261 (2020).
- [82] K. El-Badry, E. Quataert, D. R. Weisz, N. Choksi, and M. Boylan-Kolchin, *MNRAS* **482**, 4528 (2019), [arXiv:1805.03652](https://arxiv.org/abs/1805.03652) [astro-ph.GA].
- [83] M. Spera and M. Mapelli, *MNRAS* **470**, 4739 (2017), [arXiv:1706.06109](https://arxiv.org/abs/1706.06109) [astro-ph.SR].
- [84] M. Fishbach, D. E. Holz, and W. M. Farr, *The Astrophysical Journal Letters* **863**, L41 (2018).
- [85] T. Callister, M. Fishbach, D. E. Holz, and W. M. Farr, *The Astrophysical Journal Letters* **896**, L32 (2020).
- [86] Abbott et al., *Physical Review X* **11**, 021053 (2021), [arXiv:2010.14527](https://arxiv.org/abs/2010.14527) [gr-qc].
- [87] Abbott et al., *Phys. Rev. D* **109**, 022001 (2024), [arXiv:2108.01045](https://arxiv.org/abs/2108.01045) [gr-qc].
- [88] GWTC-3 samples available at <https://zenodo.org/record/5546663>.
- [89] I. Mandel, W. M. Farr, and J. R. Gair, *MNRAS* **486**, 1086 (2019), [arXiv:1809.02063](https://arxiv.org/abs/1809.02063) [physics.data-an].
- [90] M. D. Hoffman and A. Gelman, *arXiv e-prints*, [arXiv:1111.4246](https://arxiv.org/abs/1111.4246) (2011), [arXiv:1111.4246](https://arxiv.org/abs/1111.4246) [stat.CO].
- [91] R. Essick and W. Farr, *arXiv e-prints*, [arXiv:2204.00461](https://arxiv.org/abs/2204.00461) (2022), [arXiv:2204.00461](https://arxiv.org/abs/2204.00461) [astro-ph.IM].

Supplementary Material

Globular cluster simulations

We evolve a large number of globular cluster models using `cBHBd`, which includes realistic BH initial mass functions [56] and a model for the cluster formation rate and evolution through redshift [82]. We consider 25 different values of metallicity between $0.01Z_{\odot}$ and Z_{\odot} . These models follow the evolution of clusters and the formation of BH binary mergers through 3-body interactions. The BHs are paired using the pairing functions derived in [22] using Heggie’s theoretical interaction rate formulae [54]. In all models considered here we adopt an initial cluster half-mass density $\rho_h = 10^5 M_{\odot} \text{pc}^3$, and the delayed supernova mechanism [56]. When generating our model predictions, we take into account the uncertainties in the initial cluster mass density function and in the dark matter density in the Universe as in [8].

We report the results from four models that differ by the choice of the initial BH spin distribution. In one model the initial BH spins are all set to zero. Moreover, we do not include any prescription for pair-instability processes. Nevertheless, we find that no 1G BH is formed with a mass above $m_{\text{cut}} \simeq 70M_{\odot}$, implying a mass truncation set by the initial upper limit on the stellar mass function (here at $130M_{\odot}$) and by stellar wind mass-loss prior to the formation of the BHs. In a second model, we assume that the initial BH spin distribution follows a beta distribution with $\alpha = 2$ and $\beta = 18$, which peaks at $a \simeq 0.06$ and has a median at $\simeq 0.1$. In a third model, the initial BH spin distribution follows a beta distribution with $\alpha = 2$ and $\beta = 5$, which peaks at $a \simeq 0.2$ and has a median at $\simeq 0.26$. In a fourth model, we use a beta distribution with $\alpha = 2$ and $\beta = 5$, which peaks at 0.5 and has a median at 0.5. In these latter three models, $m_{\text{cut}} \simeq 51M_{\odot}$, as determined by the adopted prescriptions for pair instability [taken from 83].

In Fig. S1 we show the differential merger rate of BH binaries as a function of χ_{eff} , χ_p and m_1 . We separately plot the populations of 1G+1G mergers, 1G+2G mergers, 2G+2G mergers, and the remaining mergers that involve higher generation BHs, the majority of which are 3G+1G and 3G+2G mergers. The figure shows that the simulated populations cannot explain the peak at $10M_{\odot}$ inferred from the GW data under the POWERLAW + PEAK model from GWTC-3 [6], but can account for all mergers with primary mass $m_1 \gtrsim 30M_{\odot}$. The merger rate above the initial BH mass upper limit is dominated in all models by 1G+2G mergers. As expected based on our theoretical considerations, the left panel of Fig. S1 shows that their χ_{eff} distribution is nearly uniform (i.e., flat) within $|\chi_{\text{eff}}| < 0.5$; the distribution of χ_p is peaked at $\simeq 0.7$; and as the 1G BH spin increases, the overall contribution of 1G+2G binaries to the merger rate decreases. Naturally, 1G+2G as well as 2G+2G mergers have a null contribution to the merger rate above $m_1 > 2m_{\text{cut}}$. In this range of masses, the merging binaries are 3G+1G, 3G+2G and 4G+1G.

Fig. S2 shows χ_{eff} vs χ_p for a fraction of the binaries that merge in each model. The mean correlation between these two parameters is well described by our simple model. The model with $(\alpha, \beta) = (2, 2)$ demonstrates significant overlap in the spin parameter distributions for 1G+1G and 1G+2G mergers, while still showing a substantial merger rate contribution from 1G+2G mergers. Thus, a confidently measurable value of χ_p alone cannot be used to identify a single detected binary as hierarchically formed if BH natal spins are high. On the other hand, the population properties can be clearly used to put a hierarchical formation scenario to the test, as we do in this work.

Probability density distributions

We have previously used the cumulative distribution functions obtained from our Bayesian modeling since these can directly be used to determine the fraction of mergers that might be produced by hierarchical mergers when compared to the expected distribution. For completeness, we report in Fig. S3 the probability density functions of χ_{eff} and χ_p obtained under models $\pi_{\mathcal{N}+\mathcal{N}u_w}$ and π_{χ_p} , respectively.

Population models, data and hierarchical inference

We perform hierarchical Bayesian inferences to fit the data of the observed events with a given population model. Here, we summarise the main ingredients of the models, the data we use, and our inference analysis method.

As described in the main text, we investigate several different models for the χ_{eff} distribution of binary BHs as a function of their m_1 . These are sketched in Fig. S4. Illustrated in the left-hand subplot, models $\pi_{\mathcal{N}+u}$ and $\pi_{\mathcal{N}+u_w}$ (see equation (5)) assume that the effective spin distributions transitions from a Gaussian to a flat uniform distribution above some threshold mass \tilde{m} . Shown in the middle subplot, model $\pi_{\mathcal{N}+\mathcal{N}u_w}$ (see equation (6)) instead assumes that

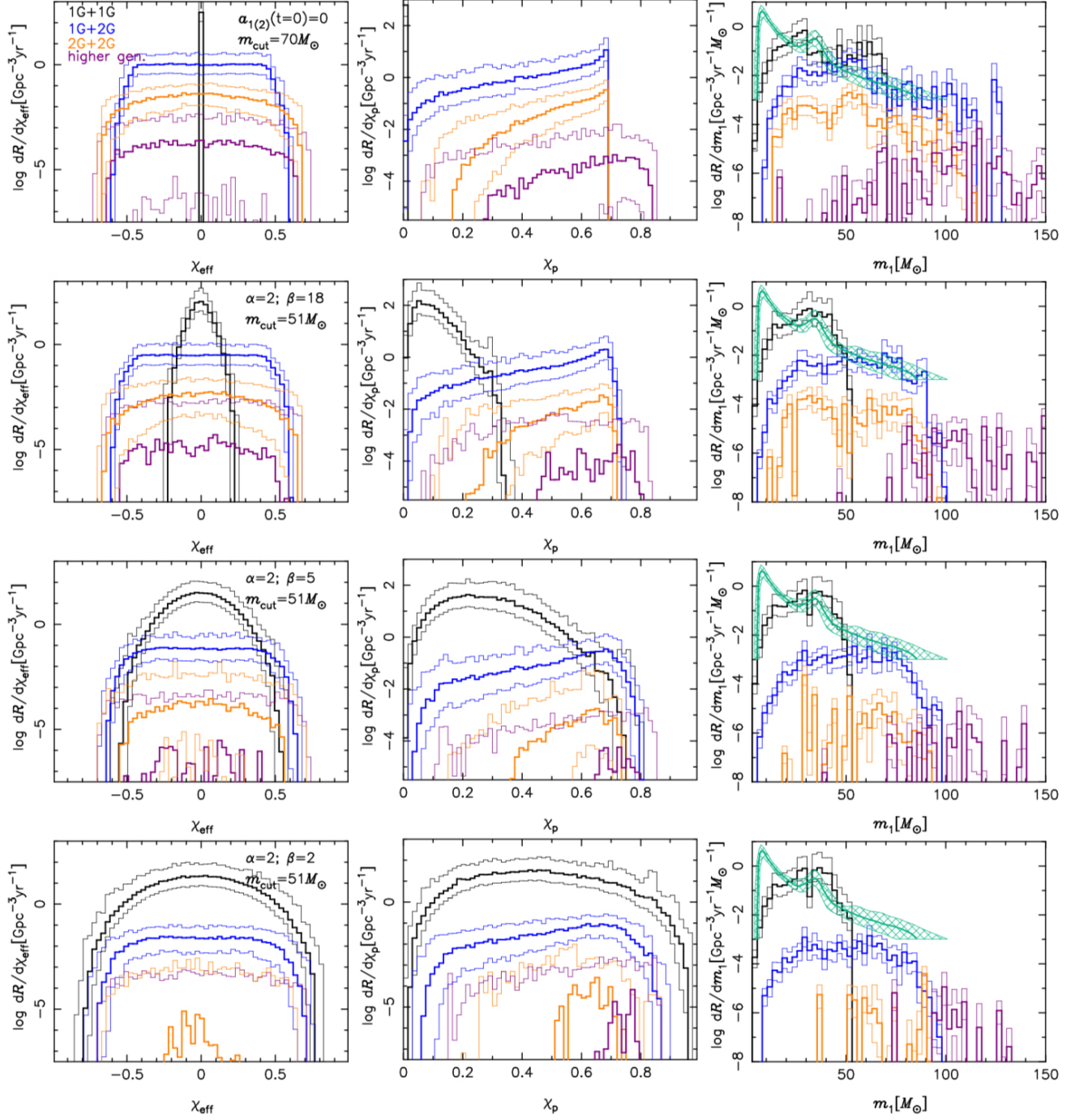


FIG. S1. Differential merger rate of BH binaries formed in globular cluster simulations as a function of binary effective spin parameters χ_{eff} (left panels), χ_p (central panels), and primary BH mass m_1 (right panels). The upper panels show the results for a model where the first generation BHs are formed with no spin, while in the other models the BH birth spins follow a beta distribution with the α and β parameters as shown. The plot gives the median value of the merger rate in each bin, together with the 95 and 5 percentiles as thinner solid lines. In the right panel the green curve and hatched regions show the mean rate and confidence intervals as reported by [6] under the POWERLAW + PEAK model.

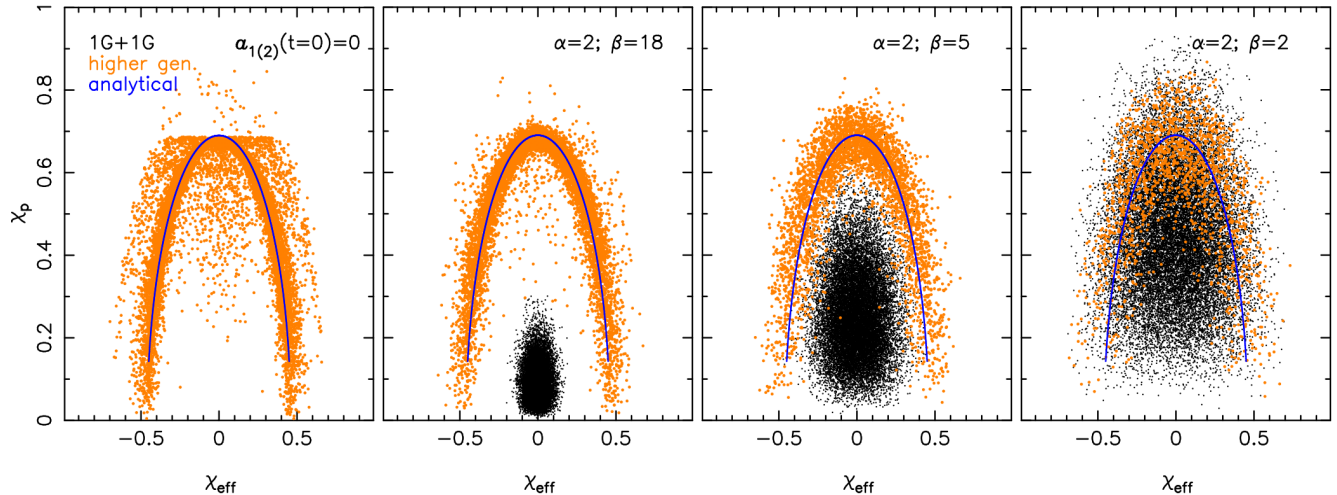


FIG. S2. Values of χ_{eff} and χ_{p} for a fraction of randomly selected binary BH mergers formed in our cluster models. The blue line shows the mean correlation predicted by our simple analytical model.

Parameter	Prior	$\mathcal{N} + \mathcal{U}$	$\mathcal{N} + \mathcal{U}_w$	$\mathcal{N} + \mathcal{N}\mathcal{U}_w$	$\mathcal{N}_m + \mathcal{U}_w$	χ_{p}
\tilde{m}	$\mathcal{U}(20, 100)$	✓	✓	✓	✓	✓
w	$\mathcal{U}(0, 1)$	–	✓	✓	✓	✓
μ	$\mathcal{U}(-1, 1)$	✓	✓	✓	✓	✓
ζ	$\mathcal{U}(0, 1)$	–	–	✓	–	–
μ_u	$\mathcal{U}(-1, 1)$	–	–	✓	–	–
$\log_{10} \sigma$	$\mathcal{U}(-1, 1)$	✓	✓	✓	✓	✓
$\log_{10} \sigma_u$	$\mathcal{U}(-1, 1)$	–	–	✓	–	–
$\delta\mu$	$\mathcal{U}(-2.5, 1)$	–	–	–	✓	–
$\delta \log \sigma$	$\mathcal{U}(-2, 1.5)$	–	–	–	✓	–
$\mu_{\text{p,u}}$ and $\mu_{\text{p,l}}$	$\mathcal{U}(0, 1)$	–	–	–	–	✓
$\log \sigma_{\text{p,u}}$ and $\log \sigma_{\text{p,l}}$	$\mathcal{U}(-1.5, 0)$	–	–	–	–	✓

TABLE S1. Priors adopted on the hyperparameters describing the effective spin distribution of binary BHs. For each parameter, we additionally indicate the model(s) in which the parameter appears.

Parameter	Prior	Defined in
β_q	$\mathcal{N}(0, 3)$	equation (S7)
κ	$\mathcal{N}(0, 6)$	equation (S8)
μ_m	$\mathcal{U}(50 M_{\odot}, 100 M_{\odot})$	equation (S4)
σ_m	$\mathcal{U}(2 M_{\odot}, 15 M_{\odot})$	equation (S4)
f_p	$\mathcal{U}(0, 1)$	equation (S4)
λ	$\mathcal{N}(-2, 3)$	equation (S4)
m_{max}	$\mathcal{U}(60 M_{\odot}, 100 M_{\odot})$	equation (S4)
m_{min}	$\mathcal{U}(5 M_{\odot}, 15 M_{\odot})$	equation (S4)
$\log_{10} dm_{\text{max}}/M_{\odot}$	$\mathcal{U}(0.5, 1.5)$	equation (S4)
$\log_{10} dm_{\text{min}}/M_{\odot}$	$\mathcal{U}(-1, 1)$	equation (S4)

TABLE S2. Priors adopted for the hyperparameters with which we describe the primary mass, mass ratio, and redshift distributions of the binary BH population.

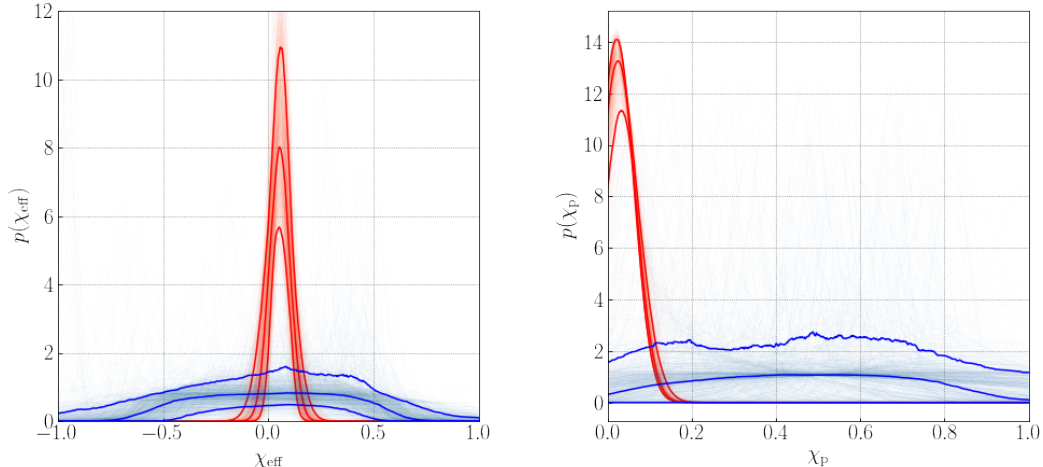


FIG. S3. Distributions of χ_{eff} and χ_p inferred using the mixture models described in the main text. The blue (red) thick lines give the median, 10th and 90th quantiles for the distribution above (below) \tilde{m} . Light lines correspond to individual draws from the posteriors.

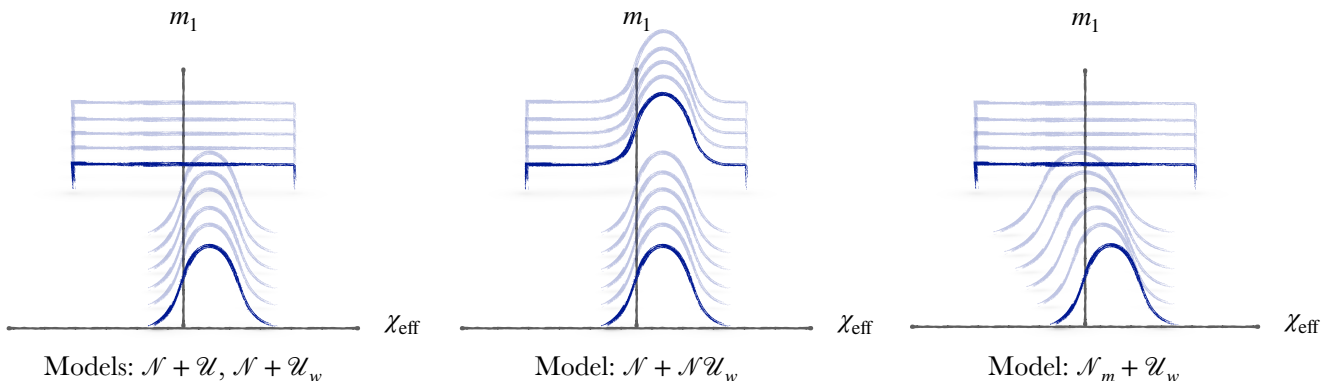


FIG. S4. Cartoon illustrating the main models examined in the main text.

the Gaussian spin distribution persists across both low- and high-mass systems, but includes a uniform component above \tilde{m} . Finally, in the right-hand panel, model $\pi_{\mathcal{N}_m + \mathcal{U}_w}$ (see equation (7)) adopts a low-mass Gaussian whose mean and log-standard deviation vary linearly as a function of mass. The priors on the hyperparameters defining each model are listed in Table S1.

We perform hierarchical inference on the binary BH population using the Hamiltonian Monte Carlo sampling algorithm implemented `numpyro`, a probabilistic programming library based on `jax`. Hamiltonian Monte Carlo methods require a likelihood that is a differentiable function of the population hyperparameters. However, the piecewise equations that define our spin models (e.g. equation (5)) are not differentiable; the discontinuities at $m_1 = \tilde{m}$ cause the likelihood to itself discontinuously as a function of \tilde{m} . To remedy this, in practice we implement these piecewise models as sharp but continuous transitions in the effective spin distributions above and below \tilde{m} . Our baseline model $\pi_{\mathcal{N} + \mathcal{U}}$ defined in equation (5), for example, is approximated as

$$\pi_{\mathcal{N} + \mathcal{U}}(\chi_{\text{eff}} | m_1) = [1 - \eta(m_1)] \mathcal{N}(\chi_{\text{eff}}; \mu, \sigma) + \eta(m_1) \mathcal{U}(\chi_{\text{eff}}; w = 0.47), \quad (\text{S1})$$

where

$$\eta(m_1) = \left[1 + \exp\left(-\frac{(m_1 - \tilde{m})}{3 M_\odot}\right) \right]^{-1} \quad (\text{S2})$$

is a logistic function that is approximately equal to zero below \tilde{m} and unity above. Other spin models are implemented analogously. Similarly, a true truncated uniform distribution at high masses would cause the likelihood to change discontinuously with w . When implementing $\mathcal{U}(\chi_{\text{eff}}; w)$ we therefore do not use an infinitely sharp truncation at the boundaries but instead exponentially suppress the distribution beyond $|\chi_{\text{eff}}| = w$:

$$\mathcal{U}(\chi_{\text{eff}}; w) \propto \begin{cases} 1 & (|\chi_{\text{eff}}| \leq w) \\ \exp\left[-\frac{(|\chi_{\text{eff}}| - w)^2}{2(0.1)^2}\right] & (|\chi_{\text{eff}}| > w). \end{cases} \quad (\text{S3})$$

Our conclusions do not depend on the precise scales over which the above smoothing takes place.

Alongside the effective spin distribution, we hierarchically measure the distribution of binary BH primary masses m_1 , mass ratios q , and redshifts z . We model the m_1 distribution as a mixture between a power law and a Gaussian, with exponential tapering functions at high and low masses:

$$p(m_1) \propto T_1(m_1)T_h(m_1)\left[(1 - f_p)P(m_1) + f_p\mathcal{N}(m_1)\right]. \quad (\text{S4})$$

Here, $P(m_1) \propto m_1^\lambda$ and $\mathcal{N}(m_1) \propto \exp\left[-\frac{(m_1 - \mu_m)^2}{2\sigma_m^2}\right]$ are power-law and Gaussian distributions, each normalized over the interval $2M_\odot \leq m_1 \leq 100M_\odot$. The tapering functions are defined as

$$T_1(m_1) = \begin{cases} \exp\left[-\frac{(m_1 - m_{\text{min}})^2}{2dm_{\text{min}}^2}\right] & (m_1 < m_{\text{min}}) \\ 1 & (m_1 \geq m_{\text{min}}) \end{cases} \quad (\text{S5})$$

and

$$T_h(m_1) = \begin{cases} 1 & (m_1 \leq m_{\text{max}}) \\ \exp\left[-\frac{(m_1 - m_{\text{max}})^2}{2dm_{\text{max}}^2}\right] & (m_1 > m_{\text{max}}) \end{cases} \quad (\text{S6})$$

We assume that the secondary mass m_2 distribution follows [32]

$$p(m_2|m_1) \propto m_2^{\beta_q} \quad (2M_\odot \leq m_2 \leq m_1). \quad (\text{S7})$$

Finally, we assume a distribution of z that is proportional to the differential comoving volume dV_c/dz , with a possible evolution in the merger rate towards higher z [84, 85]

$$p(z) \propto \frac{1}{1+z} \frac{dV_c}{dz} (1+z)^\kappa. \quad (\text{S8})$$

The priors placed on the hyperparameters governing the m_1 , q , and z distributions are listed in Table S2.

We perform our inference using the subset of binary BH events from GWTC-3 with false alarm rates below 1 yr^{-1} . We exclude GW170817, GW190425, GW190426, GW190814, GW190917, GW200105, GW200115 [7, 86], as they have at least one component with a mass $< 3M_\odot$ [6]. This leaves a total of $N_{\text{det}} = 69$ binary black holes in our sample. We use parameter estimation samples made publicly available through the [Gravitational-Wave Open Science Center](#). For events first published in GWTC-1 [5], we use the “Overall_posterior” parameter estimation samples. For events first published in GWTC-2 [86] and GWTC-2.1 [87], we adopt the “PrecessingSpinIMRHM” samples, and for events in GWTC-3 [7], we use the “C01: Mixed” samples [88]. These selections correspond to a union of samples obtained with different waveform families. All samples account for spin precession effects, while the PrecessingSpinIMRHM and C01: Mixed samples from GWTC-2, GWTC-2.1, and GWTC-3 additionally include the effects of higher order modes (parameter estimation incorporating higher order modes was not available in GWTC-1). We assess the detection efficiency using the set of successfully recovered binary BH injections, provided by the LIGO-Virgo-KAGRA collaborations, spanning their first three observing runs [57].

We perform our analysis using standard hierarchical inference. Let $p(\theta_i|d_i)$ be posteriors on the individual parameters θ_i (e.g. component masses, redshift, etc.) of each gravitational-wave event, conditioned on its observed data d_i . The corresponding posterior on the population parameters Λ is [e.g., 32, 84, 89]

$$p(\Lambda | \{d_i\}) \propto p(\Lambda) \xi^{-N_{\text{det}}}(\Lambda) \prod_{i=1}^{N_{\text{det}}} \int d\theta_i p(\theta_i|d_i) \frac{p(\theta_i|\Lambda)}{p_{\text{pe}}(\theta_i)}, \quad (\text{S9})$$

where $p_{\text{pe}}(\theta_i)$ is the prior adopted for purposes of parameter estimation and $p(\Lambda)$ is our prior on the population-level parameters. We use the priors listed in Tables S1 and S2. We replace integration over $p(\theta_i|d_i)$ with an ensemble average taken over the posterior samples associated with each event:

$$p(\Lambda | \{d_i\}) \propto p(\Lambda) \xi^{-N_{\text{det}}}(\Lambda) \prod_{i=1}^{N_{\text{det}}} \left\langle \frac{p(\theta_i|\Lambda)}{p_{\text{pe}}(\theta_i)} \right\rangle. \quad (\text{S10})$$

The detection efficiency $\xi(\Lambda)$ quantifies the total fraction of events that we expect to pass our detection criteria, given a population described by Λ . We estimate $\xi(\Lambda)$ using the injection campaign reported in [57, 87], selecting successfully found injections (with recovered false alarm rates below 1 yr^{-1} in at least one pipeline) and reweighting to the proposed population Λ as in [32]. We sample over equation (S10) using the NUMPYRO’s [79, 80] implementation of the “No U-Turn” Hamiltonian Monte Carlo algorithm [90].

The full posterior distributions on the key parameters that enter in our population analysis are given in Figs. S5, S6, S7, and S8.

We also perform several leave-one-out analyses to determine whether our results are driven primarily by a small number of unusual events. In particular, the events GW170729 and GW190517 could conceivably be driving the preference for a broad spin distribution at high masses; both events have confidently large spins ($\chi_{\text{eff}} = 0.36_{-0.25}^{+0.21}$ and $0.52_{-0.19}^{+0.20}$, respectively, under default priors) and have primary masses (50_{-10}^{+16} and $36_{-8}^{+12} M_{\odot}$) near our inferred values of w and \tilde{m} . We repeat our analysis under the $\pi_{\mathcal{N}+\mathcal{U}_w}$ model excluding one or both of GW170729 and GW190517. In all cases, results remain consistent with those shown in Fig. 2, increasing our confidence that we are identifying a feature inherent in the broader black hole population.

Finally, in order to identify possible issues due to finite sampling effects when estimating Eq. S10, we track the number of “effective samples” N_{eff} informing the Monte Carlo estimates of the likelihood for every event. Given a set of N_i posterior samples $\{\lambda_{i,j}\}_{j=1}^{N_i}$ for each event i , the $N_{\text{eff},i}$ under a proposed population Λ is

$$N_{\text{eff},i}(\Lambda) \equiv \frac{\left[\sum_{j=1}^{N_i} w_{i,j}(\Lambda) \right]^2}{\sum_{j=1}^{N_i} [w_{i,j}(\Lambda)]^2}, \quad (\text{S11})$$

where $w_{i,j}(\Lambda) = p(\lambda_{i,j}|\Lambda)/p_{\text{pe}}(\lambda_{i,j})$. Small $N_{\text{eff},i}(\Lambda) \lesssim 10$ indicates that the given event is sparsely sampled, and hence the likelihood may be dominated by sampling variance [91]. In this case, we should not necessarily trust the results of Monte-Carlo-based hierarchical inference. We do not impose any cut on $N_{\text{eff},i}(\Lambda)$. Instead, we compute and track $\min[N_{\text{eff},i}(\Lambda)]$ for each model we consider. In all cases we find that effective sample counts are large, with $\min N_{\text{eff}} > 10$ – for $\pi_{\mathcal{N}+\mathcal{U}}$, $\pi_{\mathcal{N}+\mathcal{U}_w}$, and $\pi_{\mathcal{N}+\mathcal{N}\mathcal{U}_w}$, we find $\min(\log N_{\text{eff}}) = 1.9_{-0.6}^{+0.5}$, $1.8_{-0.5}^{+0.5}$, and $1.8_{-0.4}^{+0.5}$, respectively.

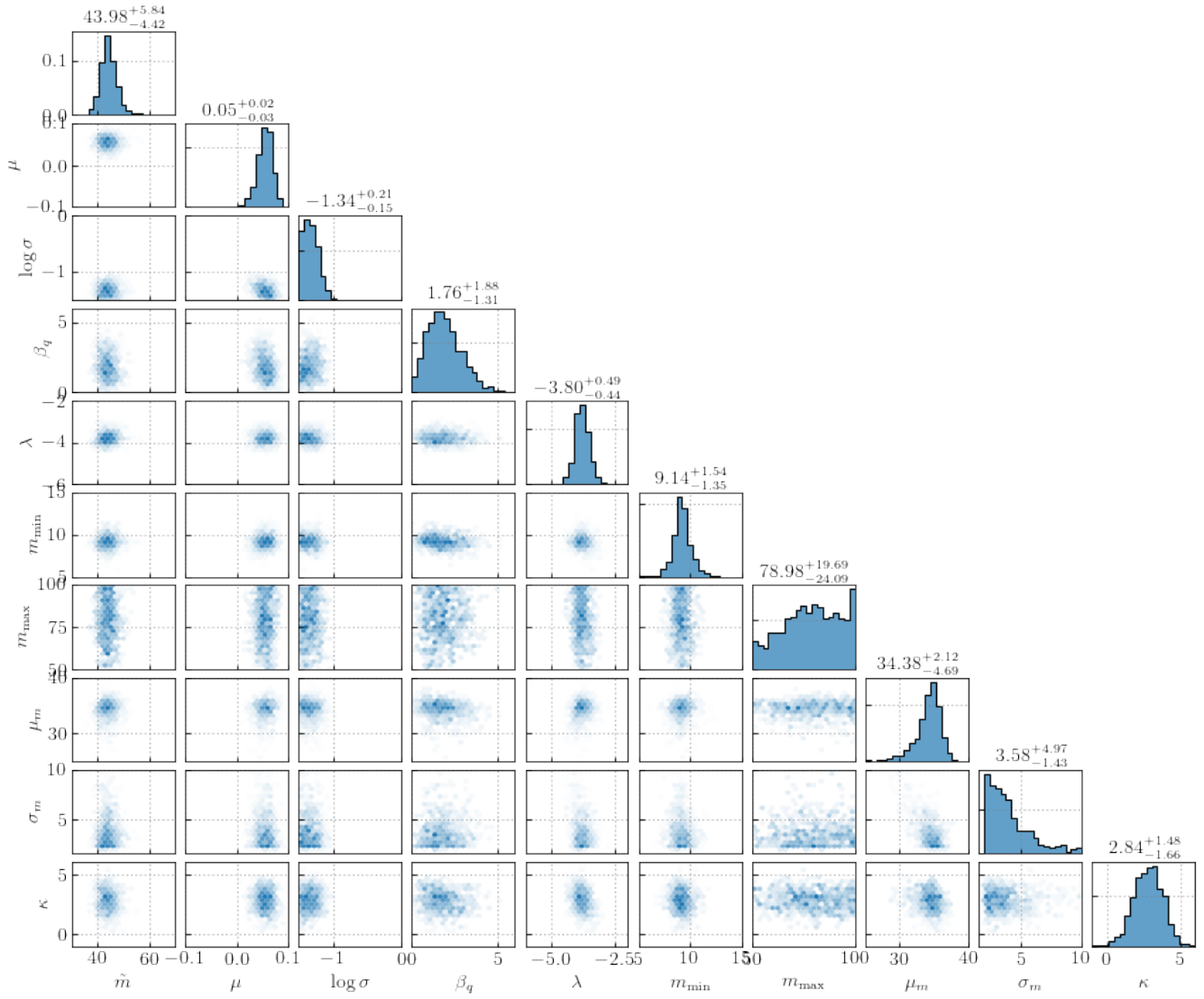


FIG. S5. Posteriors on the parameters that govern the hierarchical model where the χ_{eff} distribution is given by equation (5): a Gaussian below \tilde{m} and a Uniform distribution with half width $w = 0.47$ above \tilde{m} .

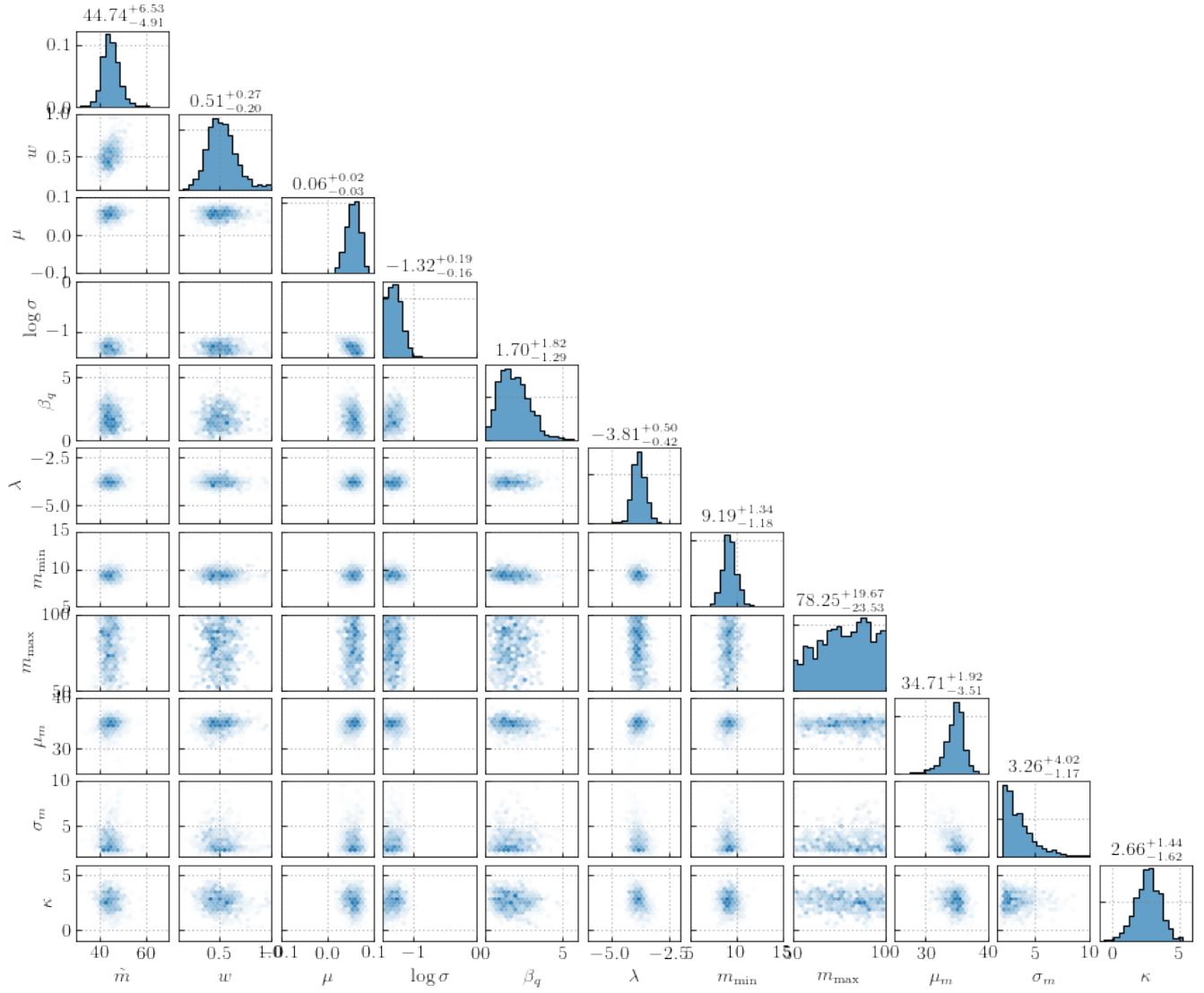


FIG. S6. Posteriors on the parameters that govern the hierarchical model where the χ_{eff} distribution is represented by a fixed Gaussian below \tilde{m} and a Uniform distribution with variable half width, w , above \tilde{m} .

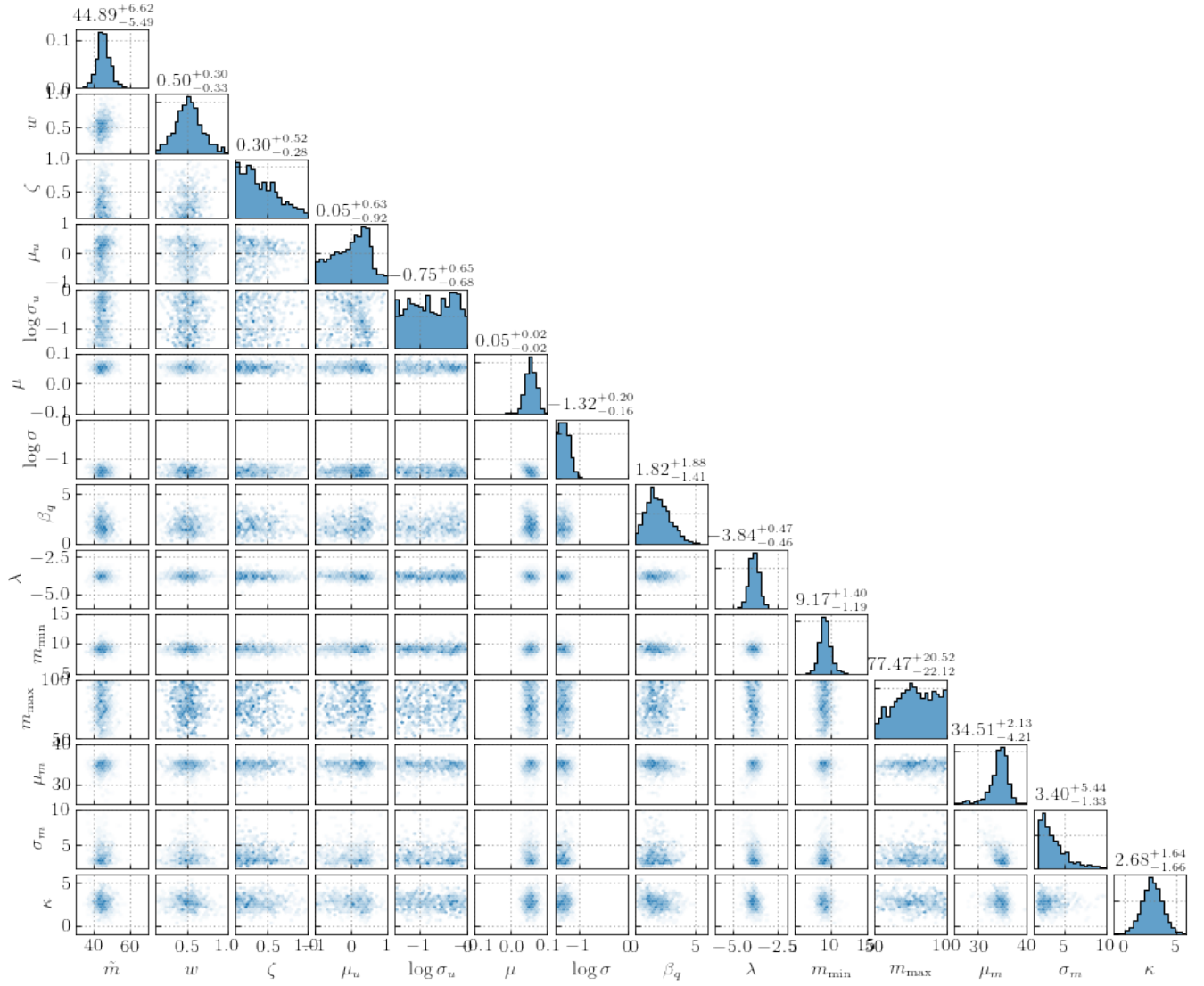


FIG. S7. Posteriors on the parameters that govern the hierarchical model where the χ_{eff} distribution is represented by equation (6): a fixed Gaussian below \tilde{m} and a Uniform distribution with variable half width, w , plus a Gaussian above \tilde{m} .

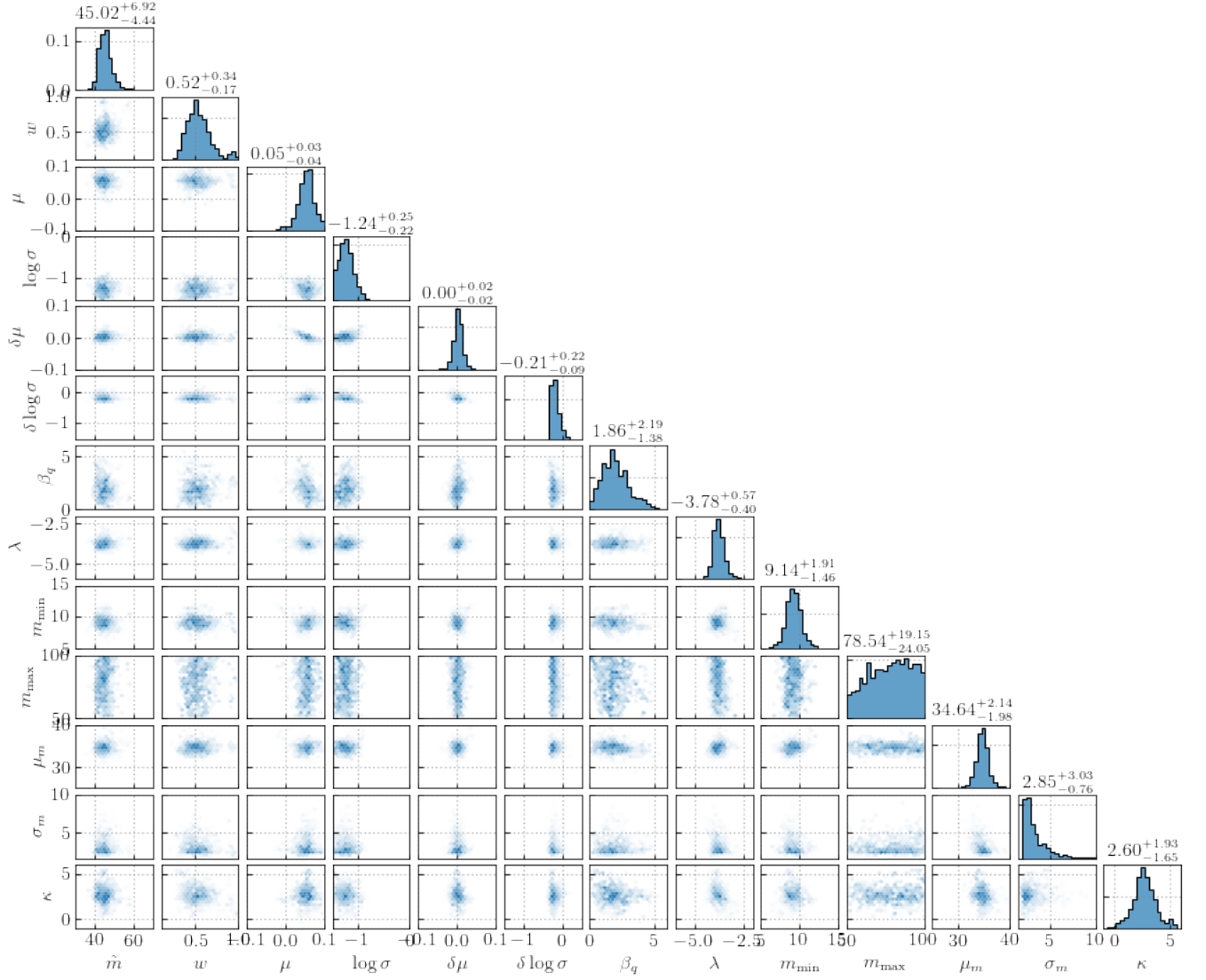


FIG. S8. Posteriors on the parameters that govern the hierarchical model where the χ_{eff} distribution is represented by equation (7): a Gaussian with mass dependent mean and variance below \tilde{m} and a fixed Uniform distribution with half width w above \tilde{m} .